



1    **Competition alters predicted forest carbon cycle responses to nitrogen availability and**  
2    **elevated CO<sub>2</sub>: simulations using an explicitly competitive, game-theoretic vegetation**  
3    **demographic model**

4

5    Ensheng Weng<sup>1,2</sup>, Ray Dybzinski<sup>3</sup>, Caroline E. Farrior<sup>4</sup>, Stephen W. Pacala<sup>5</sup>

6    <sup>1</sup>Center for Climate Systems Research, Columbia University, New York, NY 10025

7    <sup>2</sup>NASA Goddard Institute for Space Studies, 2880 Broadway, New York, NY 10025

8    <sup>3</sup>Institute of Environmental Sustainability, Loyola University Chicago, Chicago, IL 60660

9    <sup>4</sup>Department of Integrative Biology, University of Texas at Austin, Austin, TX 78712

10    <sup>5</sup>Department of Ecology & Evolutionary Biology, Princeton University, Princeton, NJ 08544

11

12    **Corresponding author:** Ensheng Weng ([wengensheng@gmail.com](mailto:wengensheng@gmail.com); phone: 212-678-5585)

13

14    **Key words:** Allocation; Biome Ecological strategy simulator (BiomeE); Competitively-optimal  
15    strategy; Game theory; Nitrogen cycle

16



17 **Abstract:** Competition is a major driver of carbon allocation to different plant tissues (e.g.  
18 wood, leaves, fine roots), and allocation, in turn, shapes vegetation structure. To improve their  
19 modeling of the terrestrial carbon cycle, many Earth system models now incorporate vegetation  
20 demographic models (VDMs) that explicitly simulate the processes of individual-based  
21 competition for light and soil resources. Here, in order to understand how these competition  
22 processes affect predictions of the terrestrial carbon cycle, we simulate forest responses to  
23 elevated CO<sub>2</sub> along a nitrogen availability gradient using a VDM that allows us to compare fixed  
24 allocation strategies versus competitively-optimal allocation strategies. Our results show that  
25 competitive- and fixed-allocation strategies predict opposite fractional allocation to fine roots  
26 and wood, though they predict similar changes in total NPP along the nitrogen gradient. The  
27 competitively-optimal allocation strategy predicts decreasing fine root and increasing wood  
28 allocation with increasing nitrogen, whereas the fixed allocation strategy predicts the opposite.  
29 Although simulated plant biomass at equilibrium increases with nitrogen due to increases in  
30 photosynthesis for both allocation strategies, the increase in biomass with nitrogen is much  
31 steeper for competitively-optimal allocation due to its increased allocation to wood. The  
32 qualitatively opposite fractional allocation to fine roots and wood of the two strategies also  
33 impacts the effects of elevated [CO<sub>2</sub>] on plant biomass. Whereas the fixed allocation strategy  
34 predicts an increase in plant biomass under elevated [CO<sub>2</sub>] that is approximately independent of  
35 nitrogen availability, competition's effect on wood allocation amplifies plant biomass under  
36 elevated [CO<sub>2</sub>] with increasing nitrogen availability. Our results indicate that the VDMs that  
37 explicitly include the effects of competition for light and soil resources on plant strategies may  
38 generate significantly different ecosystem-level predictions than those that use fixed allocation  
39 strategies.

40



## 41 **1 Introduction**

42 Allocation of assimilated carbon to different plant tissues is a fundamental aspect of plant growth  
43 and profoundly affects terrestrial ecosystem biogeochemical cycles (Cannell and Dewar, 1994;  
44 Lacoïnte, 2000). Ecologically, allocation represents an evolutionarily-honed “strategy” of plants  
45 that use limited resources and compete with other individuals and consequently drives  
46 successional dynamics and vegetation structure (De Kauwe et al., 2014; DeAngelis et al., 2012;  
47 Haverd et al., 2016; Tilman, 1988). Biogeochemically, allocation links plant physiological  
48 processes, such as photosynthesis and respiration, to biogeochemical cycles and carbon storage  
49 of ecosystems (Bloom et al., 2016; De Kauwe et al., 2014). Thus, correctly modeling allocation  
50 patterns is critical for correctly predicting terrestrial carbon cycles and Earth system dynamics.

51 In current Earth System Models (ESMs), the terrestrial carbon cycle is usually simulated by  
52 pool-based compartment models that simulate ecosystem carbon and/or nitrogen cycles as  
53 lumped pools and fluxes of plant tissues and soil organic matter (Emanuel and Killough, 1984;  
54 Eriksson, 1971; Parton et al., 1987; Randerson et al., 1997; Sitch et al., 2003). In these models,  
55 the dynamics of carbon can be described by a linear system of equations (Koven et al., 2015;  
56 Luo et al., 2001; Luo and Weng, 2011; Sierra and Mueller, 2015; Xia et al., 2013):

$$57 \quad \frac{dX}{dt} = AX + BU \quad (\text{Eq. 1})$$

58 where  $X$  is a vector of ecosystem carbon pools,  $U$  is carbon input (i.e., Gross Primary Production,  
59 GPP),  $B$  is the vector of allocation parameters to autotrophic respiration and plant carbon pools  
60 (e.g., leaves, stems, and fine roots), and  $A$  is a matrix of carbon transfer and turnover. In this  
61 system, carbon dynamics are defined by carbon input ( $U$ ), allocation ( $B$ ), and residence time and  
62 transfer coefficients ( $A$ ). The allocation schemes ( $B$ ) are thus embedded in a linear system, or



63 quasi-linear system if the allocation parameters in  $B$  are a function of carbon input ( $U$ ) or plant  
64 carbon pools ( $X$ ).

65       The modeling of allocation in this system (i.e., the parameters in vector  $B$ ) is usually based  
66 on plant allometry, biomass partitioning, and resource limitation (De Kauwe et al., 2014;  
67 Montané et al., 2017). The allocation parameters are either fixed ratios to leaves, stems, and  
68 roots, which may vary among plant functional types (e.g., CENTURY, Parton et al., 1987; TEM,  
69 Raich et al., 1991; CASA, Randerson et al., 1997) or are responsive to climate and soil  
70 conditions as a way to phenomenologically mimic the shifts in allocation that are empirically  
71 observed or hypothesized (e.g., CTEM, Arora and Boer, 2005; ORCHIDEE, Krinner et al., 2005;  
72 LPJ, Sitch et al., 2003). These modeling approaches either assume that vegetation is equilibrated  
73 (fixed ratios) or average the responses of plant types to changes in environmental conditions as a  
74 collective behavior. Thus, the carbon dynamics in these models can be constrained by selecting  
75 appropriate parameters of allocation, turnover rates, and transfer coefficients to fit the  
76 observations (Friend et al., 2007; Hoffman et al., 2017; Keenan et al., 2013).

77       To predict transient changes in vegetation structure and composition in response to climate  
78 change, vegetation demographic models (VDMs) that are able to simulate transient population  
79 dynamics are incorporated into ESMs (Fisher et al., 2018; Scheiter and Higgins, 2009).  
80 Generally, these VDMs explicitly simulate plant reproduction, growth, and mortality to generate  
81 the dynamics of populations. To speed computations and minimize complexity, groups of  
82 individuals are usually modeled as cohorts. These models may also simulate the competition  
83 between individuals for light and soil resources to drive vegetation succession and thus changes  
84 in the combinations of plant traits that represent competition strategies at different stages  
85 (Scheiter et al., 2013; Scheiter and Higgins, 2009; Weng et al., 2015). Competitively-optimal



86 allocation strategies can therefore be reasonably predicted based on the costs and benefits of  
87 allocation strategies through their effects on demographic processes (i.e., fitness) and ecosystem  
88 biogeochemical cycles (Farrion et al., 2015; Weng et al., 2015).

89 The processes of VDMs (e.g., demographic processes, individual-based competition for  
90 different resources, and community assembly) can be used to bring plant functional diversity and  
91 adaptive dynamics into ESMs, causing dominant plant traits to change in response to plant  
92 competition, environmental conditions, and ecosystem development. The dynamic response of  
93 plant traits can substantially change predictions of ecosystem biogeochemical dynamics of  
94 current ESMs since it changes the key parameters of vegetation physiological processes and soil  
95 organic matter decomposition (e.g., Dybzinski et al., 2015; Farrion et al., 2015; Weng et al.,  
96 2017). Using the methodology of adaptive dynamics, the dynamics of plant trait(s) in succession  
97 can be described by a canonical equation in a simple and continuous case (Dieckmann et al.,  
98 2007):

$$99 \frac{ds}{dt} = \frac{1}{2} \mu(s) \sigma^2(s) N(s) \frac{\partial W(s',s)}{\partial s'} \quad (\text{Eq. 2})$$

100 where,  $\mu$  is the mutation rate,  $\sigma^2$  is the variance of mutation distribution,  $N$  is the population size  
101 at equilibrium, and  $\frac{\partial W(s',s)}{\partial s'}$  is the selection gradient.  $W(s',s)$  is the fitness function, measured as  
102 the fitness of a rare individual with trait value  $s'$  (i.e., a “mutant,” “novel colonist,” “invader,” or  
103 “challenger”) in an environment created by a population of individuals with trait value  $s$  (the  
104 “resident”).

105 With such a model, the carbon dynamics of an ecosystem are the emergent result of  
106 competition among different strategies as represented by plant traits, and the most competitive  
107 strategies may shift with community composition during succession. The key parameters that are  
108 used to estimate carbon dynamics in the linear system model (Eq. 1), such as allocation ( $B$ ) and



109 residence times in different carbon pools (matrix  $A$ , which includes coefficients of carbon  
110 transfer and turnover time) become functions of competition strategies that vary with  
111 environment and carbon input. In addition, the turnover of vegetation carbon pools becomes a  
112 function of allocation and mortality rates, which change with vegetation succession and the most  
113 competitive plant traits. These changes make the system nonlinear and can lead to large biases  
114 within the framework of the compartmental pool-based models as represented by Eq. (1) (Sierra  
115 et al., 2017; Sierra and Mueller, 2015). Because of the high complexity associated with  
116 demographic and competition processes, the model predictions are usually sensitive to the  
117 parameters in these processes and are of high uncertainty (e.g., Pappas et al., 2016).

118 In contrast to their implementation in the more complicated VDMs discussed above,  
119 models of competitively-dominant plant strategies using much simpler model structures and  
120 assumptions can sometimes be solved analytically (Dybzinski et al., 2011, 2015; Farrior et al.,  
121 2013, 2015). Although simplified, such models can pin-point the key processes that improve the  
122 predictive power of simulation models (Dybzinski et al., 2011; Farrior et al., 2013, 2015),  
123 allowing them to help researchers formulate model processes and understand the simulated  
124 ecosystem dynamics in ESMs. For example, the analytical model derived by Farrior et al. (2013)  
125 that links interactions between ecosystem carbon storage, allocation, and water stress at elevated  
126  $\text{CO}_2$  sheds light on the otherwise inscrutable processes leading to varied soil water dynamics in a  
127 land model coupled with an VDM (Weng et al., 2015). Recognizing the benefit, Weng et al.  
128 (2017) included both a simplified analytical model and a more complicated VDM to understand  
129 competitively optimal leaf mass per area, competition between evergreen and deciduous plant  
130 functional types, and the resulting successional patterns.



131           In this study, we use a stand-alone simulator derived from the LM3-PPA model (Weng et  
132 al., 2017, 2015) to show how forests respond to elevated CO<sub>2</sub> and nitrogen availability via  
133 different competitively-optimal allocation strategies. The model is an individual-based  
134 vegetation demographic model, whose vegetation demographic scheme has been coupled into the  
135 land model of the Geophysical Fluid Dynamical Laboratory's Earth System Model (Shevliakova  
136 et al., 2009; Weng et al., 2015) and NASA Goddard Institute for Space Study's Earth system  
137 model, ModelE (Schmidt et al., 2014). Using this model, we simulate the shifts in competitively  
138 optimal allocation strategies in response to elevated CO<sub>2</sub> at different nitrogen levels based on  
139 insights from the analytical model derived by Dybzinski et al. (2015). Dybzinski et al.'s (2015)  
140 model predicts that increases in carbon storage at elevated CO<sub>2</sub> relative to storage at ambient  
141 CO<sub>2</sub> are largely independent of total nitrogen because of an increasing shift in carbon allocation  
142 from long-lived, low-nitrogen wood to short-lived, high-nitrogen fine roots under elevated CO<sub>2</sub>  
143 with increasing nitrogen availability. Here, we analyze the simulated ecosystem carbon cycle  
144 variables (gross and net primary production, allocation, and biomass) of separate fixed-allocation  
145 and competitively-optimal allocation model runs. In the fixed-allocation runs, ecosystem  
146 properties are the result of the prescribed allocation strategies of a given PFT, analogous to the  
147 fixed allocation schemes of most VDMs (see above). In the competitively-optimal allocation  
148 runs, competition between the different allocation strategies results in succession and the  
149 eventual dominance of the most competitive allocation strategy for a given nitrogen availability  
150 and CO<sub>2</sub> level. Since everything else in the model is identical, we are able to compare the  
151 predictions of fixed-allocation strategies with competitively-optimal allocation strategies by  
152 comparing the ecosystem properties of these two types of runs.



## 153 2 Methods and Materials

### 154 2.1 BiomeE Model

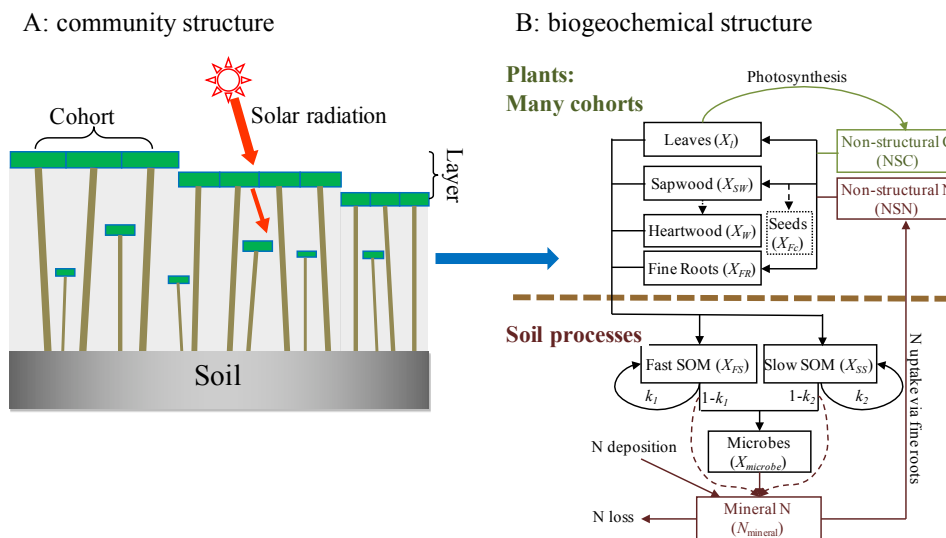
155 We used a stand-alone ecosystem simulator (Biome Ecological strategy simulator,  
156 BiomeE) to conduct simulation experiments. BiomeE is derived from the version of LM3-PPA  
157 used in Weng *et al.* (2017). We simplified the processes of energy transfer and soil water  
158 dynamics of LM3-PPA (Weng *et al.*, 2015) but still retained the key features of plant physiology  
159 and individual-based competition for light, soil water, and, via the decomposition of soil organic  
160 matter, nitrogen (Fig. 1). In this model, individual trees are represented as sets of *cohorts* of  
161 similar size trees and are arranged in different vertical canopy layers according to their height  
162 and crown area following the rules of the Perfect Plasticity Approximation (PPA) model (Strigul  
163 *et al.*, 2008). Sunlight is partitioned into these canopy layers according to Beer's law. Thus, a key  
164 parameter for light competition, critical height, is defined; all the trees above this context-  
165 dependent height get full sunlight and all trees below this height are shaded by the upper layer  
166 trees. Plant growth, reproduction, and mortality are driven by the carbon assimilation of leaves,  
167 which is in turn dependent on water and nitrogen uptake by fine roots.

168 Each tree consists of seven pools: leaves, fine roots, sapwood, heartwood, fecundity  
169 (seeds), and non-structural carbohydrates and nitrogen (NSC and NSN, respectively) (Fig. 1: b).  
170 The carbon and nitrogen in plant pools enter the soil pools with the mortality of individual trees  
171 and the turnover of leaves and fine roots. There are three soil organic matter (SOM) pools for  
172 carbon and nitrogen: fast-turnover, slow-turnover, and microbial pools, along with a mineral  
173 nitrogen pool for mineralized nitrogen in soil. The simulation of SOM decomposition and  
174 nitrogen mineralization is based on the models of Gerber *et al.* (2010) and Manzoni *et al.* (2010)  
175 and described in detail in Weng *et al.* (2017). The decomposition rate of a SOM pool is





176 determined by the basal turnover rate together with soil temperature and moisture. The nitrogen  
 177 mineralization rate is a function of decomposition rate and the C:N ratio of the SOM. Microbes  
 178 must consume more carbon in the high C:N ratio SOM pool to get enough nitrogen and must  
 179 release excessive nitrogen in the low C:N ratio SOM pool to get enough carbon for energy  
 180 (Weng *et al.* 2017).  
 181



182

183 **Figure 1. Model structure of BiomeE**

184 Panel A: vegetation structure: trees organize their crowns into canopy layers according to both  
 185 their height and their crown area following the rules of the PPA model, which mechanistically  
 186 models light competition. Panel B: Biogeochemical structure and compartmental pools. The  
 187 green, brown, and black lines are the flows of carbon, nitrogen, and coupled carbon and nitrogen,  
 188 respectively. The green box is for carbon only. The brown boxes are N pools. The black boxes  
 189 are for both carbon and nitrogen pools, where  $X$  can be C (carbon) and N (nitrogen). The C:N  
 190 ratios of leaves, fine roots, seeds, and microbes are fixed. The C:N ratios of woody tissues, fast  
 191 soil organic matter (SOM), and slow SOM are flexible. Only one tree's C and N pools are shown  
 192 in this figure. The model can have multiple cohorts of trees, which share the same pool structure.  
 193 The dashed line separates the plant and soil processes.



194

195 **Nitrogen uptake** The rate of nitrogen uptake ( $U$ ,  $\text{g N m}^{-2} \text{ hour}^{-1}$ ) from the soil mineral  
 196 nitrogen pool is an asymptotically increasing function of fine root biomass density ( $Root_{\text{total}}$ ,  $\text{kg C}$   
 197  $\text{m}^{-2}$ ), following McMurtrie *et al.* (2012)

$$U = f_{U,\text{max}} \cdot N_{\text{mineral}} \cdot \frac{Root_{\text{total}}}{Root_{\text{total}} + Root_0}, \quad (\text{Eq. 3})$$

198 where,  $N_{\text{mineral}}$  is the mineral N in soil ( $\text{g N m}^{-2}$ ),  $f_{U,\text{max}}$  is the maximum rate of nitrogen  
 199 absorption per hour when  $Root_{\text{total}}$  approaches infinity,  $Root_0$  is a constant of root biomass ( $\text{kg C}$   
 200  $\text{m}^{-2}$ ) at which the nitrogen uptake rate is half of the parameter  $f_{U,\text{max}}$ . The nitrogen uptake rate  
 201 of an individual tree ( $U_{\text{tree}}$ ,  $\text{g N hour}^{-1} \text{ tree}^{-1}$ ) is calculated as follows:

$$U_{\text{tree}} = U \cdot \frac{Root_{\text{tree}}}{Root_{\text{total}}}, \quad (\text{Eq. 4})$$

202 where,  $Root_{\text{tree}}$  is the fine root biomass of a tree ( $\text{kg C tree}^{-2}$ ). The N absorbed by roots enters into  
 203 the NSN pool and then is allocated to plant tissues through plant growth following carbon flows.

204 **Allocation** Carbon assimilated by leaves via photosynthesis enters into the NSC pool first  
 205 and is subsequently used for respiration, growth, and reproduction. The partitioning of carbon  
 206 and nitrogen into the plant pools (*i.e.*, leaves, fine roots, and sapwood) is limited by a set of  
 207 allometric equations and the C:N ratios of these pools. Empirical allometric equations relate  
 208 woody biomass (including coarse roots, bole, and branches), crown area, and stem diameter. The  
 209 individual-level dimensions of a tree, *i.e.*, height ( $Z$ ), biomass ( $S$ ), and crown area ( $A_{\text{CR}}$ ) are  
 210 given by empirical allometries (Dybzinski *et al.*, 2011; Farrior *et al.*, 2013):

$$\begin{aligned} Z(D) &= \alpha_Z D^{\theta_Z} \\ S(D) &= 0.25\pi\Lambda\rho_W\alpha_Z D^{2+\theta_Z} \\ A_{\text{CR}}(D) &= \alpha_c D^{\theta_c} \end{aligned} \quad (\text{Eq. 5})$$



211 where  $Z$  is tree height,  $S$  is total woody biomass carbon (including bole, coarse roots, and  
 212 branches) of a tree,  $\alpha_c$  and  $\alpha_z$  are PFT-specific constants,  $\theta_c=1.5$  and  $\theta_z=0.5$  (Farrior et al.,  
 213 2013) (although they could be made PFT-specific if necessary),  $\pi$  is the circular constant,  $\lambda$  is a  
 214 PFT-specific taper constant, and  $\rho_w$  is PFT-specific wood density ( $\text{kg C m}^{-3}$ ).

215 We set *targets* for leaf, fine root, and sapwood cross-sectional area that govern plant  
 216 allocation of non-structural carbon and nitrogen during growth. These *targets* are related by the  
 217 following equations based on the assumption of the pipe model (Shinozaki, Kichiro et al., 1964):

$$\begin{aligned}
 L_k^*(D, p) &= l_k^* \cdot A_{CR}(D) \cdot LMA \cdot p(t) \\
 FR_k^*(D) &= \varphi_{RL} \cdot l_k^* \cdot \frac{A_{CR}(D)}{SRA} \\
 A_{SW,k}^*(D) &= \alpha_{CSA} \cdot l_k^* \cdot A_{CR}(D)
 \end{aligned}
 \tag{Eq. 6}$$

218 where  $L_k^*(D, p)$  is the target leaf mass of canopy-level  $k$  at given stem diameter ( $D$ ),  $l_k^*$  is the  
 219 target leaf area per unit crown area of a given PFT at canopy-level  $k$ ,  $A_{CR}(D)$  is the crown area of  
 220 a tree with diameter  $D$ , LMA is PFT-specific leaf mass per unit area, and  $p(t)$  is a PFT-specific  
 221 function ranging from zero to one that governs leaf phenology (Weng et al., 2015). Note, here  
 222  $\varphi_{RL}$  is fixed for each PFT and will remain so for the fixed allocation strategies and the  
 223 competitive allocation strategies. The process of choosing a context-dependent competitive  
 224 dominant  $\varphi_{RL}$  will take place after finding the fitness of each  $\varphi_{RL}$  in monoculture and in  
 225 competition with other PFTs (*i.e.*, different values of  $\varphi_{RL}$ ). The phenology function  $p(t)$  takes  
 226 values 0 (non-growing season) or 1 (growing season) following the phenology model of LM3-  
 227 PPA (Weng et al., 2015). The onset of a growing season is controlled by two variables, growing  
 228 degree days (GDD), and a weighted mean daily temperature ( $T_{pheno}$ ), while the end of a growing  
 229 season is controlled by  $T_{pheno}$ .  $FR_k^*(D)$  is the target fine root biomass at tree diameter  $D$  and  
 230 canopy-level  $k$ ,  $\varphi_{RL}$  is the target ratio of total root surface area to the total leaf area, SRA is



231 specific root area,  $A_{SW,k}^*(D)$  is the target cross sectional area of sapwood at canopy-level  $k$ , and  
 232  $\alpha_{CSA}$  is an empirical constant (the ratio of sapwood cross-sectional area to target leaf area).

233 In the model simulation, plant growth is updated at a daily time step. For each simulated  
 234 day, the model calculates the amount of carbon and nitrogen that are available for growth (i.e.,  
 235 building new tissues) according to the total NSC and NSN and current leaf and fine root  
 236 biomass. Basically, the available NSC ( $NSC_g$ ) is the summation of a small fraction of the total  
 237 NSC in an individual plant and the differences between the targets of leaf and fine roots and their  
 238 current biomass capped by a larger fraction of NSC (Eq. 7).

$$NSC_g = \min(f_1 NSC, f_2 NSC + L^* + FR^* - L - FR), \quad (\text{Eq. 7})$$

239 where  $L^*$  and  $FR^*$  are the targets of leaves and fine roots, respectively, and functions of plant size  
 240 (see Eq. 6);  $L$  and  $FR$  are current leaf and fine roots biomass. The parameters  $f_1$  and  $f_2$  give the  
 241 daily availability of NSC during periods of leaf flush at the beginning of a growing season and  
 242 normal growth after plant leaves and fine roots approach their targets. Usually, parameter  $f_1$  is  
 243 much greater than  $f_2$ . We let  $f_1=0.05$  and  $f_2= 1/(365 \times 3)$  in this study. The equation for available  
 244 NSN is analogous.

245 The allocation of the available NSC and NSN to wood, leaves, fine roots, and seeds is  
 246 calculated in four steps. 1) First, the model allocates a small fraction of the available NSC (0.15  
 247 in this study) for sapwood growth. 2) Then it allocates to leaves and fine roots by tracking PFT-  
 248 specific targets for leaf area per unit crown area ( $l^*$ ) and the ratio of fine root area per to leaf area  
 249 ( $\phi_{RL}$ ). As long as there are sufficient available NSC and NSN, plants allocate them to new leaves  
 250 and fine roots to close the gap between their current and target areas. 3) If there are extra  
 251 available NSC and NSN left after the leaves and fine roots reached their targets, they will be



252 allocated to sapwood and seeds. Since the C:N ratios of leaves, fine roots, and seeds are fixed in  
253 this model, the nitrogen used to construct these tissues is simply the carbon allocated from NSC  
254 to them divided by their leaf C:N ratio, respectively. 4) When the available NSN cannot meet the  
255 demand, the excess carbon is re-allocated to sapwood because sapwood requires less nitrogen  
256 than those of leaves, fine roots, and seeds at the same supply of carbon.

257       Based on these allocation rules, the mean of allocations of carbon and nitrogen to leaves,  
258 fine roots, and wood over a growing season are governed by the targets for the leaf area per unit  
259 crown area (i.e., crown leaf area index,  $l^*$ ) and fine root area per unit leaf area ( $\phi_{RL}$ ). Since the  
260 crown leaf area index,  $l^*$ , is fixed in this study,  $\phi_{RL}$  is the key parameter determining the relative  
261 allocation of carbon to fine roots and stems. A high  $\phi_{RL}$  means a high relative allocation to fine  
262 roots and therefore low relative allocation to stems, and *vice versa*.

## 263 **2.2 Site and Data**

264 Data pertaining to vegetation, climate, and soil at Harvard Forest (Aber et al., 1993; Hibbs, 1983;  
265 Urbanski et al., 2007) were used to design the plant functional types (PFTs) and ecosystem  
266 nitrogen levels used in the simulation experiments, to drive the model, and to calibrate model  
267 parameters. Harvard Forest is located in Massachusetts, USA (42.54°, -72.17°). The climate of  
268 Harvard Forest is cool temperate with annual precipitation 1050 mm, distributed fairly evenly  
269 throughout the year. The annual mean temperature is 8.5 °C with a high monthly mean  
270 temperature of 20°C in July and a low of -7°C in January. The soils are mainly sandy loam with  
271 average depth around 1 m and are moderately well drained in most areas. The vegetation is  
272 deciduous broadleaf/mixed forest with major species red oak (*Quercus rubra*), red maple (*Acer*  
273 *rubrum*), black birch (*Betula lenta*), white pine (*Pinus strobus*), and hemlock (*Tsuga canadensis*)  
274 (Compton and Boone, 2000; Savage et al., 2013). The data used to drive our model runs are gap-



275 filled hourly meteorological data at Harvard Forest from 1991 to 2006, obtained from North  
276 American Carbon Program (NACP) Site-Level Synthesis datasets (Barr et al., 2013).

### 277 **2.3 Simulation experiments**

278 We set two atmospheric CO<sub>2</sub> concentration ([CO<sub>2</sub>]) levels: 380 ppm and 580 ppm, and  
279 eight ecosystem total nitrogen levels (ranging from 114.5 gN m<sup>-2</sup> to 552 gN m<sup>-2</sup> at the interval of  
280 62.5 gN m<sup>-2</sup>) for our simulation experiments (Table 1). In all the simulation experiments, we  
281 assume there are no nitrogen inputs or outputs to the system. The nitrogen cycles through the  
282 plant and soil pools and is redistributed among them via plant demographic processes, soil  
283 carbon transfers, and plant uptake. The PFTs were based on a PFT of an evergreen needle-leaved  
284 tree with different leaf to fine root area ratios,  $\varphi_{RL}$ , in the range from 1 to 8 (Table 1). Simply  
285 stated, the PFTs we investigate only differ in parameter  $\varphi_{RL}$ .

286 We define the model runs initialized with only one fixed- $\varphi_{RL}$  PFT as “fixed-allocation  
287 runs” although the actual allocation of carbon to different plant tissues varies with [CO<sub>2</sub>]  
288 concentration and ecosystem nitrogen availability. We define the model runs initialized with  
289 multiple PFTs as “competition runs” (eight PFTs with different  $\varphi_{RL}$  at the beginning, although  
290 many are driven to extinction during a given model run). We conducted one set of fixed-  
291 allocation runs and two sets of competition runs (Table 1).

292 In the fixed-allocation runs, we run the full factorial combinations of the eight PFTs with  
293 root/leaf area ratios ( $\varphi_{RL}$ ) from 1 to 8 and the eight ecosystem total nitrogen levels (Table 1), but  
294 only those with  $\varphi_{RL} \leq 6$  survived at ambient CO<sub>2</sub> (380 ppm) because the carbon consumed by  
295 fine roots exceeded what leaves provided at high  $\varphi_{RL}$ . The fixed allocation runs are for exploring  
296 the model predictions of gross primary production (GPP), net primary production (NPP),



297 allocation, and biomass at equilibrium with fixed root/leaf area ratios ( $\varphi_{RL}$ ) and ecosystem total  
 298 nitrogen levels, analogous to the fixed allocation schemes used in many VDMs.

299

300

**Table 1 Simulation experiments**

Type	Model runs	Initial PFT(s) $\varphi_{RL}$	Ecosystem total nitrogen levels	CO <sub>2</sub> concentration [CO <sub>2</sub> ]
Fixed- allocation runs	One model run per combination of PFT ( $\varphi_{RL}$ ), nitrogen level, and CO <sub>2</sub> concentration	One of the following PFTs: $\varphi_{RL} = 1, 2, 3, 4, 5, 6,$ 7, or 8	Eight levels ranging from 114.5 g N m <sup>-2</sup> to 552 g N m <sup>-2</sup> at the interval of 62.5 g N m <sup>-2</sup> : 114.5 g N m <sup>-2</sup> , 177 g N m <sup>-2</sup> , 239.5 g N m <sup>-2</sup> , 302 g N m <sup>-2</sup> , 364.5 g N m <sup>-2</sup> , 427 g N m <sup>-2</sup> , 489.5 g N m <sup>-2</sup> , 552 g N m <sup>-2</sup>	Ambient: 380 ppm  Elevated: 580 ppm
Competition runs I	One model run per combination of nitrogen level and CO <sub>2</sub> concentration	All the PFTs ( $\varphi_{RL} =$ 1~ 8) used in the fixed-allocation runs		
Competition runs II	One model run per combination of nitrogen level and CO <sub>2</sub> concentration	Eight PFTs with $\varphi_{RL}$ ranging from 4.5-0.5 <i>i</i> to 8.5-0.5 <i>i</i> at the interval of 0.5, where <i>i</i> denotes the eight nitrogen levels from 114.5 to 552 gN m <sup>-2</sup> .		

301

302 In competition runs I, we used the same PFTs as in the fixed-allocation runs, where their  
 303  $\varphi_{RL}$  varies from 1 to 8 at the interval of 1.0 and the ecosystem total nitrogen levels are the same  
 304 as those used in the fixed-allocation runs (Table 1). This set of competition runs was used to  
 305 explore successional patterns at both ambient and elevated CO<sub>2</sub> concentrations (380 ppm and  
 306 580 ppm, respectively). However, this set of model runs could not show the details of  
 307 equilibrium plant biomass and allocation patterns along the nitrogen gradient because of the  
 308 large intervals between the  $\varphi_{RL}$  values.



309 To achieve greater resolution in our competition predictions, we designed the competition  
310 runs II using a dynamic PFT combination scheme according to the ranges of  $\varphi_{RL}$  obtained from  
311 the competition runs I that could survive at a particular nitrogen level at both  $\text{CO}_2$   
312 concentrations. For each nitrogen level, we set eight PFTs with  $\varphi_{RL}$  that varied in a range 3.5  
313 (e.g.,  $x \sim x+3.5$ ) at the interval of 0.5, starting with the highest  $\varphi_{RL}$  of 8.0 at the lowest N level  
314 ( $114.5 \text{ gN m}^{-2}$ ) and decreasing 0.5 per level of increase in ecosystem total N. Let  $i=1, 2, \dots, 8$   
315 denote the eight N levels from 114.5 to  $552 \text{ gN m}^{-2}$ , the  $\varphi_{RL}$  of the eight PFTs at each level are  
316 ( $5.0-0.5i, 5.5-0.5i, \dots, 8.5-0.5i$ ) (Table 1). For example, at the nitrogen of  $114.5 \text{ gN m}^{-2}$  ( $i = 1$ ),  
317 the  $\varphi_{RL}$  of the eight PFTs are 4.5, 5.0, ..., 8.0 and at  $177 \text{ gN m}^{-2}$  ( $i = 2$ ), they are 4.0, 4.5, ..., 7.5.

318 For both fixed-allocation and competition runs, visual inspection indicated that stands had  
319 reached equilibrium after  $\sim 1200$  years. To be conservative, we present equilibrium data by  
320 averaging model properties between years 1400 and 1800. We compared simulated equilibrium  
321 gross primary production (GPP), net primary production (NPP), allocation (both absolute amount  
322 of carbon and fractions of the total NPP), and plant biomass of the competition runs II with those  
323 from the fixed-allocation runs. We used the results from one PFT ( $\varphi_{RL}=4$ ) to highlight the  
324 differences of plant responses with competitively optimal allocation strategies. The complete  
325 results from the fixed-allocation runs are shown in the Figures S1 and S2 in supplementary  
326 materials.

### 327 **3 Results**

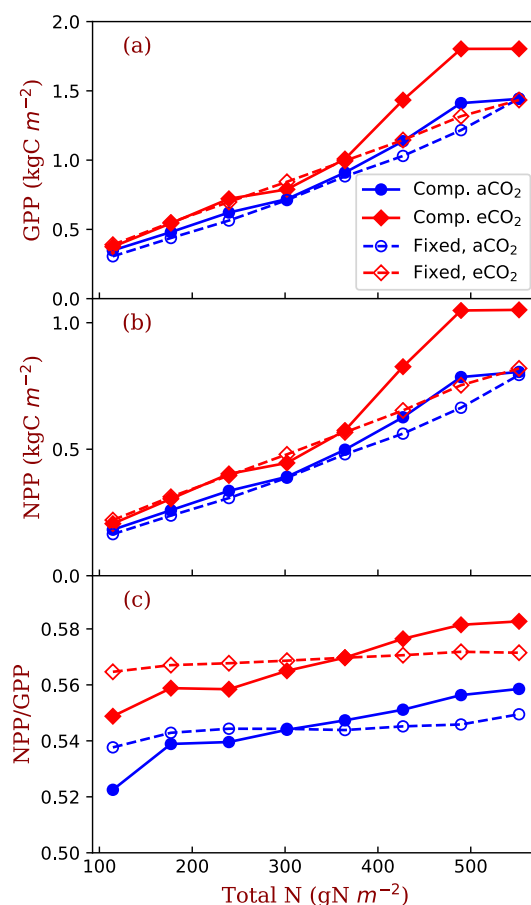
328 In the competition runs, the equilibrium GPP and NPP increase with total nitrogen at values  
329 similar to those of the fixed-allocation runs (Fig. 2: a and b). However, the  $\text{CO}_2$  stimulation of  
330 NPP increases with total nitrogen in competition runs more than it in the fixed-allocation runs.  
331 Elevated  $[\text{CO}_2]$  increases carbon use efficiency (defined as the ratio of NPP to GPP in this study,





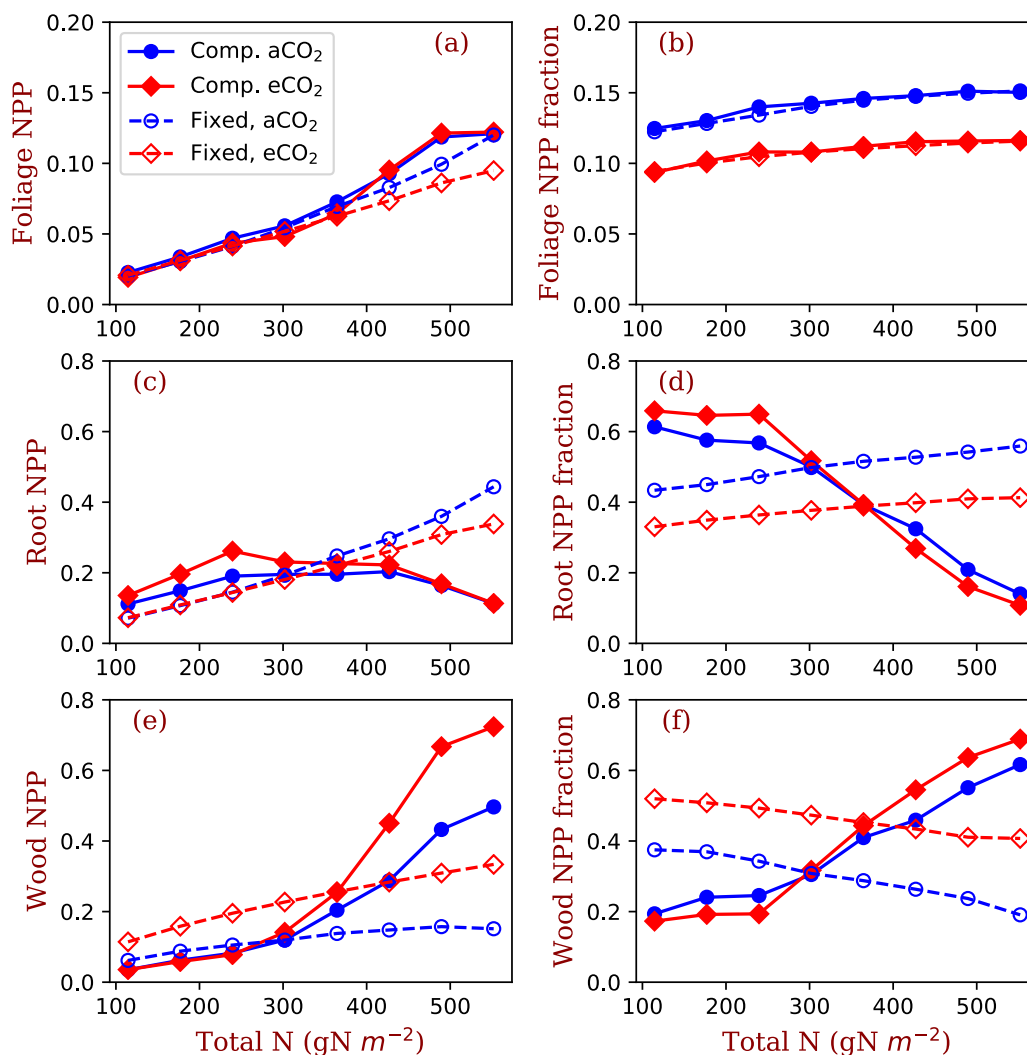
332 NPP/GPP) in both the fixed-allocation and competition runs (Fig. 2: c). Also, the dependence of  
333 NPP/GPP on nitrogen is higher in the competition runs than it in the fixed-allocation runs.

334



335

336 **Figure 2 Equilibrium Gross Primary Production (GPP, a), Net Primary Production (NPP,**  
337 **b), and Carbon Use Efficiency (NPP/GPP, c).** The closed symbols with solid line represent  
338 competition runs (comp.). The open symbols with dashed lines represent fixed-allocation runs  
339 (only  $\varphi_{RL}=4$  shown in this figure).



340

341 **Figure 3** Allocation to leaves, fine roots, and wood tissues of the competition and fixed-  
 342 allocation runs at the eight total nitrogen levels and two CO<sub>2</sub> concentrations. The panels a, c, and  
 343 e show the NPP allocated to the tissues and the panels b, d, and f show the fractions of the  
 344 allocation in total NPP. The closed symbols with solid line represent competition runs (comp.).  
 345 The open symbols with dashed lines represent fixed-allocation runs (only  $\varphi_{RL}=4$  shown in this  
 346 figure).

347

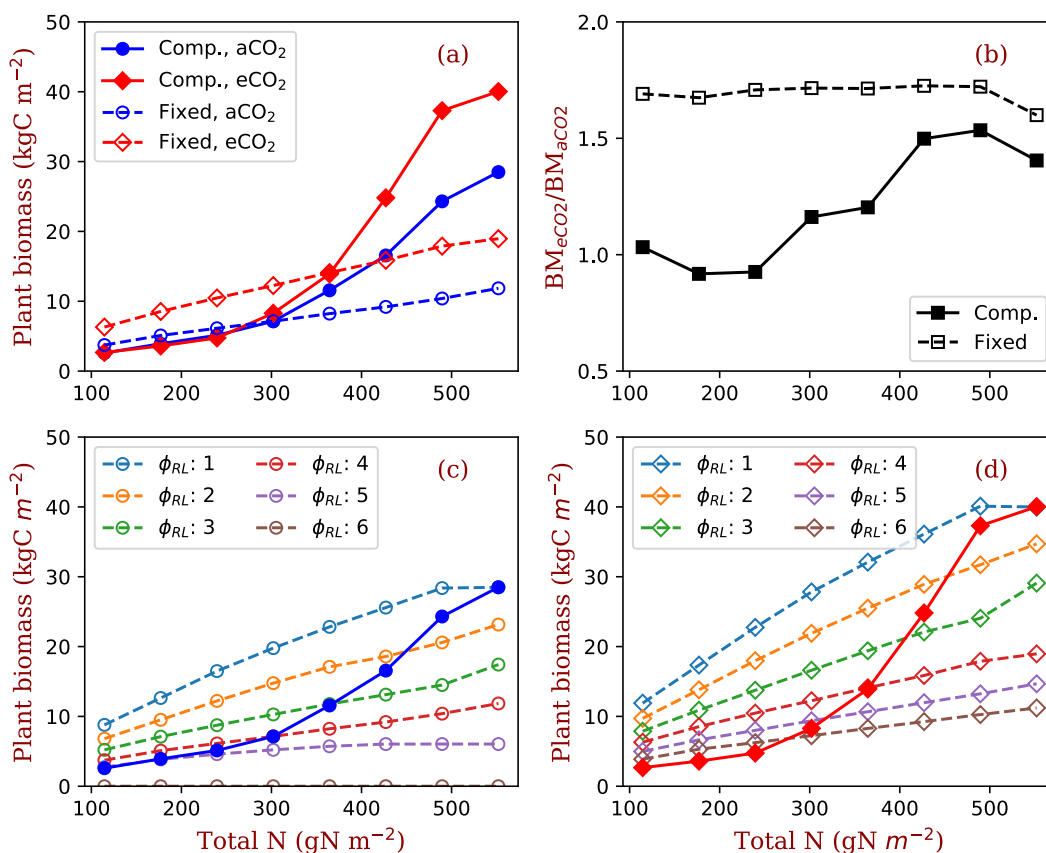


348 Allocation of NPP to leaves increases with total nitrogen in all conditions, i.e. both  
349 competition and fixed-allocation at both ambient  $[\text{CO}_2]$  and elevated  $[\text{CO}_2]$  (Fig. 3: a). Foliage  
350 NPP is similar in these four model runs when N is low. At high nitrogen ( $>400 \text{ g N m}^{-2}$ ),  
351 competition runs have higher foliage NPP than the fixed-allocation runs generally. Allocation to  
352 leaves is relatively stable across the nitrogen gradient at the two  $\text{CO}_2$  concentration levels (Fig. 3:  
353 b). The fraction of NPP allocated to leaves changes little with nitrogen (Fig. 3: b) and it is  
354 universally higher at ambient  $[\text{CO}_2]$  than at elevated  $[\text{CO}_2]$ .

355 Allocation of NPP to fine roots is hump-shaped with increasing nitrogen in competition  
356 runs, whereas it increases monotonically with increasing nitrogen in fixed-allocation runs (Fig. 3:  
357 c). Elevated  $[\text{CO}_2]$  increases fine root allocation at low nitrogen in competition runs but  
358 decreases root allocation irrespective of nitrogen in fixed-allocation runs (Fig. 3: c). The fraction  
359 of NPP allocated to fine roots decreases with nitrogen at both  $\text{CO}_2$  concentrations in competition  
360 runs but it increases slightly in fixed-allocation runs (Fig. 3: d). In fixed-allocation runs, elevated  
361  $\text{CO}_2$  reduces the fraction of NPP allocated to fine roots at all nitrogen levels. In competition runs,  
362 fractional allocation to fine roots increases at elevated  $[\text{CO}_2]$  when ecosystem total nitrogen is  
363 low (e.g.,  $114.5 - 302 \text{ g N m}^{-2}$ ) and decrease at elevated  $[\text{CO}_2]$  when ecosystem total nitrogen is  
364 high (e.g.,  $364-552 \text{ g N m}^{-2}$ ).

365 In the reverse of the fine root response, NPP allocation to woody tissues increases with  
366 total nitrogen in both competition and fixed-allocation runs (Fig. 3: e). In competition runs, the  
367 fraction of allocation to woody tissues decreases at elevated  $[\text{CO}_2]$  when ecosystem total  
368 nitrogen is low (e.g.,  $114 - 245 \text{ g N m}^{-2}$ ) and increases at elevated  $[\text{CO}_2]$  when ecosystem total  
369 nitrogen is high (e.g.,  $302 - 552 \text{ g N m}^{-2}$ ).

370



371

372

**Figure 4 Plant biomass responses to elevated  $[\text{CO}_2]$  and nitrogen**

373 Panel a shows the equilibrium plant biomass (means of simulated plant biomass from model run

374 year 1400 to 1800) in competition runs and fixed-allocation runs ( $\phi_{\text{RL}}=4$ ). Panel b shows the

375 ratio of simulated plant biomass at elevated  $[\text{CO}_2]$  to ambient  $[\text{CO}_2]$  for both competition and

376 fixed-allocation runs. Panels c and d show the comparisons with fixed-allocation runs with  $\phi_{\text{RL}}$

377 from 1 to 6 at ambient (c) and elevated  $[\text{CO}_2]$  (d). The closed symbols with solid line represent

378 competition runs. The open symbols with dashed lines represent fixed-allocation runs ( $\phi_{\text{RL}}$

379 ranges from 1 to 6).

380

381



382 As a result of the changes in competitively-optimal allocation, plant biomass increases  
383 dramatically with ecosystem nitrogen in competition runs compared with that in fixed-allocation  
384 runs (Fig. 4: a). The effects of elevated  $[\text{CO}_2]$  on plant biomass increase with nitrogen in  
385 competition runs but are constant overall in fixed-allocation runs (Fig. 4: b). Compared with the  
386 full spread of fixed-allocation runs with  $\varphi_{\text{RL}}$  ranging from 1 to 6, competition runs have high root  
387 allocation at low nitrogen and low root allocation at high nitrogen due to changes in the  
388 dominant competitive allocation strategy, which amplifies plant biomass responses to elevated  
389  $[\text{CO}_2]$  with increasing nitrogen (Fig. 4: c and d).

390 Generally, in the fixed-allocation runs, GPP and NPP increase by a factor of three along  
391 the gradient of nitrogen used in this study ( $114.5 - 552 \text{ g N m}^{-2}$ ) at both ambient and elevated  
392  $[\text{CO}_2]$  (Figs. S1 and S2). As  $\varphi_{\text{RL}}$  increases (i.e. more fine roots per unit leaf), GPP and NPP  
393 decrease at all the nitrogen levels overall, though not monotonically. The magnitude of  
394 differences in GPP and NPP due to differences in fixed allocation within a given nitrogen level is  
395 comparable to the magnitude of differences in GPP and NPP due to nitrogen level within a given  
396 fixed allocation strategy (Fig. S1: a and b) when  $\varphi_{\text{RL}}$  is in the range that allows plants to grow  
397 normally (1~5 in the case of ambient  $[\text{CO}_2]$ ). At  $\varphi_{\text{RL}}=6$ , the simulated trees just barely survive  
398 with very limited growth, and their GPP and NPP are close to zero. As prescribed by the  
399 definition of  $\varphi_{\text{RL}}$ , allocation of NPP to fine roots increases with  $\varphi_{\text{RL}}$  in fixed-allocation runs (Fig.  
400 S1: c). As a consequence, allocation of NPP to wood decreases as  $\varphi_{\text{RL}}$  increases (Fig. S1: d).  
401 Allocation to leaves does not change much with  $\varphi_{\text{RL}}$ . (Fig. S1: e, note differences in scale).  
402 Correspondingly, plant biomass at equilibrium decreases with  $\varphi_{\text{RL}}$  and almost falls to zero at  
403  $\varphi_{\text{RL}}=6$ . Total nitrogen affects the allocation to fine roots and wood (Fig. S1: d) because extra  
404 carbon is diverted to woody tissues in our model when nitrogen is limited. However, the



405 amplitude of changes in GPP and NPP induced by nitrogen availability is lower than the  
406 amplitude of changes resulting from different values of  $\varphi_{RL}$  in the fixed-allocation runs.

## 407 **4 Discussion**

### 408 **4.1 Mechanisms of model predictions**

409 In our model, the simulation of competition for light and soil resources is based on two  
410 fundamental mechanisms: 1) competition for light is based on the height of trees according to the  
411 rules of the PPA model (Strigul et al., 2008); and 2) individual nitrogen uptake is linearly  
412 dependent on the fine root surface area of an individual tree relative to that of its neighbors  
413 (Dybziński et al., 2019; McMurtrie et al., 2012; Weng et al., 2017). These two mechanisms  
414 define an allocational tradeoff between wood and fine roots for carbon and nitrogen investment  
415 in different  $[\text{CO}_2]$  and nitrogen environments. Allowing competition for these resources to  
416 determine the dominant traits results in very different predicted allocation patterns – and thus  
417 ecosystem level responses – than those of fixed allocation strategies. For example, fractional  
418 wood allocation increases with increasing nitrogen availability under competitive allocation but  
419 decreases – the opposite qualitative response – under fixed allocation (Fig. 3: f). Consequently,  
420 equilibrium plant biomass is predicted to increase much more with increasing nitrogen  
421 availability under a competitive- than under a fixed-allocation strategy (Fig. 4: c, d). In nature,  
422 the effects of competition on dominant plant traits may occur through species replacement or  
423 community assembly (akin to the mechanism in our model), but it may also occur through  
424 adaptive plastic responses or in-place sub-population evolution of ecotypes.

425 Although the strategy that maximizes the growth rate in a fixed-allocation strategy  
426 allocates very little to fine roots (Figs. S1 and S2), the competitively optimal strategy allocates  
427 more carbon to fine roots to compete for nitrogen, a competitive effect termed “fine-root



428 overproliferation” (McNickle and Dybzinski, 2013). Elevated [CO<sub>2</sub>] increases the carbon gain of  
429 leaves, making more carbon available for nitrogen competition and thus exacerbating the fine-  
430 root overproliferation (Dybzinski et al., 2015). Changes in the height at which understory trees  
431 transition to the canopy from low nitrogen to high nitrogen indicate a shift from the importance  
432 of competition for soil nitrogen to the importance of competition for light as ecosystem nitrogen  
433 increases (Fig. S3).

434 Under competitive allocation, increases in NPP and plant biomass across the nitrogen  
435 gradient are greater than the increases in NPP and plant biomass under fixed allocation (Fig. S1)  
436 because the most competitive type shifts from high fine root allocation to low fine root allocation  
437 as ecosystem total nitrogen increases from 117 to 552 g N m<sup>-2</sup> (Figs. S4 and S5). This greatly  
438 reduces the carbon cost of belowground competition. The slight decrease in the fraction of NPP  
439 allocated to leaves at elevated [CO<sub>2</sub>] occurs because of increases in total NPP and constant  
440 absolute NPP allocation to foliage. It is consistent with free air CO<sub>2</sub> enhancement (FACE)  
441 experiments that show leaf area index (LAI) in closed-canopy forests is not responsive to  
442 elevated [CO<sub>2</sub>] (Norby et al., 2003).

443 Because most nitrogen uptake is via mass flow and diffusion and because both of these  
444 mechanisms depend on sink strength, individuals with *relatively* greater fine root mass than their  
445 neighbors take a greater share of nitrogen, as was recently demonstrated empirically (Dybzinski  
446 et al., 2019). This is consistent with the idea mentioned above that fine roots may overproliferate  
447 for competitive reasons relative to lower optimal fine root mass in the hypothetical absence of an  
448 evolutionary history of competition (Craine, 2006; McNickle and Dybzinski, 2013). The  
449 increased fitness (*i.e.*, reproductive success) of the *relatively* greater strategy increases the  
450 *absolute* fine root mass. But again, individuals with even *relatively* greater fine root mass take a



451 greater share of nitrogen, leading to what has been termed a “tragedy of the commons” (Gersani  
452 et al., 2001). At high soil nitrogen, height-structured competition for light (also a game-theoretic  
453 tragedy of the commons, Falster and Westoby, 2003; Givnish, 1982) prevails, and trees with  
454 greater *relative* allocation to trunks prevail. The balance between these two competitive priorities  
455 can be observed in our model predictions as a shift from fine root allocation to wood allocation  
456 as soil nitrogen increases. This may also explain why root C:N ratio is highly variable  
457 (Dybzinski et al., 2015; Luo et al., 2006; Nie et al., 2013): a high density of fine roots in soil may  
458 be more important than the high absorption ability of a single root in competing for soil nitrogen  
459 in the usually low mineral nitrogen soils.

460 Our model predicts that the ratio of plant biomass under elevated [CO<sub>2</sub>] relative to plant  
461 biomass under ambient [CO<sub>2</sub>] should increase with increasing nitrogen due to the shift of carbon  
462 allocation from fine roots to woody tissues. In contrast, the analytic model of Dybzinski *et al.*  
463 (2015) predicts that the ratio of plant biomass under elevated [CO<sub>2</sub>] relative to plant biomass  
464 under ambient [CO<sub>2</sub>] should be largely independent of total nitrogen because of an increasing  
465 shift in carbon allocation from long-lived, low-nitrogen wood to short-lived, high-nitrogen fine  
466 roots under elevated [CO<sub>2</sub>] and with increasing nitrogen. This significant difference between  
467 these two predictions traces back to differences in how fine root stoichiometry is handled in the  
468 two models. In the model of Dybzinski *et al.* (2015), the fine root C:N ratio is flexible and the  
469 marginal nitrogen uptake capacity per unit of carbon allocated to fine roots depends on its  
470 nitrogen concentration. Like the model presented here, the model of Dybzinski *et al.* (2015)  
471 predicts decreasing fine root mass with increasing nitrogen availability. *Unlike* the model  
472 presented here (which has constant fine root nitrogen concentration), the model of Dybzinski et  
473 al. (2015) predicts increasing fine root nitrogen concentration with increasing nitrogen





474 availability. As a result, there is less nitrogen to allocate to wood as nitrogen increases in the  
475 model of Dybzinski *et al.* (2015) than there is in the model presented here. These countervailing  
476 factors even out the ratio of plant biomass under elevated [CO<sub>2</sub>] relative to plant biomass under  
477 ambient [CO<sub>2</sub>] across the nitrogen gradient in Dybzinski *et al.* (2015), whereas their absence  
478 amplifies this ratio with increasing nitrogen in the model presented here. Our ability to diagnose  
479 and understand this discrepancy highlights the utility of deploying closely-related analytical and  
480 simulation models (Weng *et al.*, 2017). It also points to a critical empirical research gap: which  
481 model's fine root (and strictly speaking, active root, McCormack *et al.*, 2017) assumptions about  
482 stoichiometry are closer to the truth?

#### 483 **4.2 Model complexity and uncertainty**

484         Compared with the conventional pool-based vegetation models that use pools and fluxes  
485 to represent plant demographic processes at a land simulation unit (e.g., grid or patch), VDMs  
486 add two new mechanisms. The first mechanism is the inclusion of stochastic birth and mortality  
487 processes of individuals (i.e., demographic processes). These processes allow the models to  
488 predict population dynamics and transient vegetation structure, such as size-structured  
489 distribution and crown organization (e.g., Moorcroft *et al.*, 2001; Strigul *et al.*, 2008). With  
490 changes in vegetation structure, allocation and mortality rates can change, generating a different  
491 carbon storage accumulation curve compared with those predicted by pool-based models where  
492 vegetation structure is not explicitly represented (e.g., Weng *et al.*, 2015). The second new  
493 mechanism is the simulated shift in dominant plant traits during succession due to shifting  
494 competitive outcomes among different PFTs, which changes the allocation between fast- and  
495 slow-turnover pools and thus the parameters of allocation and the residence time of carbon in the  
496 ecosystem.



497 Together, these mechanisms may alter long-term predictions of terrestrial carbon cycling  
498 due to changes in PFT-based parameters (Dybzinski et al., 2011; Farrior et al., 2013; Weng et al.,  
499 2015). As described in the Introduction, current pool-based models can be described by a linear  
500 system of equations characterized by the key parameters of allocation, residence time, and  
501 transfer coefficients (Eq. 1) with the rigid assumption of unchangeable plant types (Luo et al.,  
502 2012; Xia et al., 2013). In VDMs however, allocation, residence time, leaf traits, phenology,  
503 mortality, plant forms, and their responses to climate change are all strategies of competition  
504 whose success varies with the environmental conditions and the traits of the individuals they are  
505 competing against. To make predictions of carbon cycle responses to the novel conditions of  
506 climate change, we must understand what determines the most competitive strategy, how the  
507 most competitive strategy changes with conditions, and how the most competitive strategy  
508 impacts the carbon cycle.

509 Many trade-offs between plant traits can shift in response to environmental and biotic  
510 changes, limiting the applicability of varying a single trait, as we have in this study. For example,  
511 allocation, leaf traits, mycorrhizal types, and nitrogen fixation can all change with ecosystem  
512 nitrogen availability (Menge et al., 2017; Ordoñez et al., 2009; Phillips et al., 2013; Vitousek et  
513 al., 2013). The unrealistic effects of model simplification can be corrected by adding important  
514 tradeoffs that are missing. For example, the positive feedback between root allocation and SOM  
515 decomposition plays a role in mitigating the effects of tragedies of the commons of root over-  
516 proliferation (e.g., Gersani et al., 2001; Zea-Cabrera et al., 2006) due to a negative feedback  
517 induced by root turnover. High root allocation increases the decomposition rate of SOM and the  
518 supply of mineral nitrogen because of the high turnover rate of root litter, which favors a strategy  
519 of high wood allocation and reduces the competitive optimal fine root allocation. This negative



520 feedback indicates that the model structure is flexible and that we can incorporate correct  
521 mechanisms step by step to improve model prediction skills. Testing single strategies is still a  
522 necessary step to improving our understanding of the system and prediction skills of the models,  
523 though it could lead to unrealistic responses sometimes.

#### 524 **4.3 Implications for Earth system modeling**

525 In this study, we set forth a hypothesis for the tradeoffs between light competition and  
526 nitrogen uptake via allocation based on insights gained from the simpler model of Dybzinski et  
527 al. (2015) to predict allocation as an emergent property of competition. One advantage of  
528 building a model in this way is that the vegetation dynamics are predicted from first principles,  
529 rather than based on the correlations between vegetation properties and environmental  
530 conditions. For vegetation models designed to predict the effects of climate change, the  
531 important operational distinction is that the fundamental rules cannot or will not change as  
532 climate changes. Nor, presumably, will the underlying ecological and evolutionary processes  
533 change as climate changes. The emergent properties can change as climate changes however, and  
534 the models built on the “scale-appropriate” unbreakable constraints and ecological and  
535 evolutionary processes will be able to accurately predict changes in emergent ecosystem  
536 properties.

537 This modeling approach also demands improvement in model validation and benchmarking  
538 systems (Collier et al., 2018; Hoffman et al., 2017). As shown in this study, allocation responses  
539 to elevated CO<sub>2</sub> at different nitrogen levels in fixed-allocation runs are opposite to those in  
540 competitive-allocation runs. For example, in fixed-allocation runs, elevated [CO<sub>2</sub>] increases  
541 wood allocation and decreases fine root allocation at low nitrogen; whereas in competitive-  
542 allocation runs elevated [CO<sub>2</sub>] leads to low wood allocation and high fine root allocation. Simply



543 calibrating against short-term observational data may improve the agreements with observations  
544 but would not change model predictions because these results emerge from the fundamental  
545 assumptions of the models. An updated model benchmarking system should have the metrics of  
546 competitive plant traits during the development of ecosystems and their responses to changes in  
547 climate.

## 548 **5 Conclusions**

549 Overall, our study illustrates that including the competition processes for light and soil  
550 resources in a game-theoretic vegetation demographic model can substantially change the  
551 prediction of the contribution of ecosystems to the global carbon cycle. Allowing the model to  
552 track the competitive allocation strategies can generate significantly different ecosystem-level  
553 predictions than those of fixed allocation strategies. Building such a model requires  
554 differentiating between the unbreakable tradeoffs of plant traits and ecological processes from  
555 the emergent properties of ecosystems. Drawing on insights from closely-related analytical  
556 models to develop and understand more complicated simulation models seems, to us,  
557 indispensable. Evaluating these models also requires an updated model benchmarking system  
558 that includes the metrics of competitive plant traits during the development of ecosystems and  
559 their responses to climate changes.

560

## 561 **Acknowledgements**

562 This work was supported by NASA Modeling, Analysis, and Prediction (MAP) Program  
563 (NNH16ZDA001N-MAP), USDA Forest Service Northern Research Station (Agreement 13-JV-



564 11242315-066) and Princeton Environment Institute. C.E.F acknowledges support from the  
565 University of Texas at Austin.

566

567 **Codes and data availability**

568 The codes of the BiomeE model are available at GitHub:

569 <https://github.com/wengsheng/BiomeESS>

570 The simulated data from simulation experiments and Python scripts used in this study will be  
571 made publicly available at the publish of this paper.

572

573 **Reference**

- 574 Aber, J. D., Magill, A., Boone, R., Melillo, J. M. and Steudler, P.: Plant and Soil Responses to  
575 Chronic Nitrogen Additions at the Harvard Forest, Massachusetts, *Ecol. Appl.*, 3(1), 156–  
576 166, doi:10.2307/1941798, 1993.
- 577 Arora, V. K. and Boer, G. J.: A parameterization of leaf phenology for the terrestrial ecosystem  
578 component of climate models, *Glob. Change Biol.*, 11(1), 39–59, doi:10.1111/j.1365-  
579 2486.2004.00890.x, 2005.
- 580 Barr, A. G., Ricciu, D. M., Schaefer, K., Richarson, A., Agarwal, D., Thornton, P. E., Davis, K.,  
581 Jackson, B., Cook, R. B., Hollinger, D. Y., Van Ingen, C., Amiro, B., Andrews, A.,  
582 Arain, M. A., Baldocchi, D., Black, T. A., Bolstad, P., Curtis, P., Desai, A., Dragoni, D.,  
583 Flanagan, L., Gu, L., Katul, G., Law, B. E., Lafleur, P. M., Margolis, H., Matamala, R.,  
584 Meyers, T., McCaughey, J. H., Monson, R., Munger, J. W., Oechel, W., Oren, R., Roulet,  
585 N. T., Torn, M. and Verma, S. B.: NACP Site: Tower Meteorology, Flux Observations  
586 with Uncertainty, and Ancillary Data, , doi:10.3334/ornldaac/1178, 2013.
- 587 Bloom, A. A., Exbrayat, J.-F., van der Velde, I. R., Feng, L. and Williams, M.: The decadal state  
588 of the terrestrial carbon cycle: Global retrievals of terrestrial carbon allocation, pools, and  
589 residence times, *Proc. Natl. Acad. Sci.*, 113(5), 1285–1290,  
590 doi:10.1073/pnas.1515160113, 2016.
- 591 Cannell, M. G. R. and Dewar, R. C.: Carbon Allocation in Trees: a Review of Concepts for  
592 Modelling, in *Advances in Ecological Research*, vol. 25, pp. 59–104, Elsevier., 1994.
- 593 Collier, N., Hoffman, F. M., Lawrence, D. M., Keppel-Aleks, G., Koven, C. D., Riley, W. J.,  
594 Mu, M. and Randerson, J. T.: The International Land Model Benchmarking (ILAMB)  
595 System: Design, Theory, and Implementation, *J. Adv. Model. Earth Syst.*, 10(11), 2731–  
596 2754, doi:10.1029/2018MS001354, 2018.
- 597 Compton, J. E. and Boone, R. D.: Long-Term Impacts of Agriculture on Soil Carbon and  
598 Nitrogen in New England Forests, *Ecology*, 81(8), 2314, doi:10.2307/177117, 2000.
- 599 Craine, J. M.: Competition for Nutrients and Optimal Root Allocation, *Plant Soil*, 285(1–2),  
600 171–185, doi:10.1007/s11104-006-9002-x, 2006.
- 601 De Kauwe, M. G., Medlyn, B. E., Zaehle, S., Walker, A. P., Dietze, M. C., Wang, Y.-P., Luo, Y.,  
602 Jain, A. K., El-Masri, B., Hickler, T., Wårlind, D., Weng, E., Parton, W. J., Thornton, P.  
603 E., Wang, S., Prentice, I. C., Asao, S., Smith, B., McCarthy, H. R., Iversen, C. M.,  
604 Hanson, P. J., Warren, J. M., Oren, R. and Norby, R. J.: Where does the carbon go? A  
605 model-data intercomparison of vegetation carbon allocation and turnover processes at  
606 two temperate forest free-air CO<sub>2</sub> enrichment sites, *New Phytol.*, 203(3), 883–899,  
607 doi:10.1111/nph.12847, 2014.
- 608 DeAngelis, D. L., Ju, S., Liu, R., Bryant, J. P. and Gourley, S. A.: Plant allocation of carbon to  
609 defense as a function of herbivory, light and nutrient availability, *Theor. Ecol.*, 5(3), 445–  
610 456, doi:10.1007/s12080-011-0135-z, 2012.
- 611 Dieckmann, U., Brannstrom, A., HilleRisLambes, R. and Ito, H. C.: The Adaptive Dynamics of  
612 Community Structure, in *Mathematics for Ecology and Environmental Sciences*, edited  
613 by Takeuchi, Yasuhiro, Iwasa, Yoh, and Sato, Kazunori, pp. 145–177, Springer., 2007.



- 614 Dybzinski, R., Farrior, C., Wolf, A., Reich, P. B. and Pacala, S. W.: Evolutionarily Stable  
615 Strategy Carbon Allocation to Foliage, Wood, and Fine Roots in Trees Competing for  
616 Light and Nitrogen: An Analytically Tractable, Individual-Based Model and Quantitative  
617 Comparisons to Data, *Am. Nat.*, 177(2), 153–166, doi:10.1086/657992, 2011.
- 618 Dybzinski, R., Farrior, C. E. and Pacala, S. W.: Increased forest carbon storage with increased  
619 atmospheric CO<sub>2</sub> despite nitrogen limitation: a game-theoretic allocation model for trees  
620 in competition for nitrogen and light, *Glob. Change Biol.*, 21(3), 1182–1196,  
621 doi:10.1111/gcb.12783, 2015.
- 622 Dybzinski, R., Kelvakis, A., McCabe, J., Panock, S., Anuchitlertchon, K., Vasarhelyi, L., Luke  
623 McCormack, M., McNickle, G. G., Poorter, H., Trinder, C. and Farrior, C. E.: How are  
624 nitrogen availability, fine-root mass, and nitrogen uptake related empirically?  
625 Implications for models and theory, *Glob. Change Biol.*, doi:10.1111/gcb.14541, 2019.
- 626 Emanuel, W. R. and Killough, G. G.: Modeling terrestrial ecosystems in the global carbon cycle  
627 with Shifts in carbon storage capacity by land-use change, *Ecology*, 65(3), 970–983,  
628 doi:10.2307/1938069, 1984.
- 629 Eriksson, E.: Compartment Models and Reservoir Theory, *Annu. Rev. Ecol. Syst.*, 2(1), 67–84,  
630 doi:10.1146/annurev.es.02.110171.000435, 1971.
- 631 Falster, D. and Westoby, M.: Plant height and evolutionary games, *TRENDS Ecol. Evol.*, 18(7),  
632 337–343, doi:10.1016/S0169-5347(03)00061-2, 2003.
- 633 Farrior, C. E., Dybzinski, R., Levin, S. A. and Pacala, S. W.: Competition for Water and Light in  
634 Closed-Canopy Forests: A Tractable Model of Carbon Allocation with Implications for  
635 Carbon Sinks, *Am. Nat.*, 181(3), 314–330, doi:10.1086/669153, 2013.
- 636 Farrior, C. E., Rodriguez-Iturbe, I., Dybzinski, R., Levin, S. A. and Pacala, S. W.: Decreased  
637 water limitation under elevated CO<sub>2</sub> amplifies potential for forest carbon sinks, *Proc.*  
638 *Natl. Acad. Sci. U. S. A.*, 112(23), 7213–7218, doi:10.1073/pnas.1506262112, 2015.
- 639 Fisher, R. A., Koven, C. D., Anderegg, W. R. L., Christoffersen, B. O., Dietze, M. C., Farrior, C.  
640 E., Holm, J. A., Hurtt, G. C., Knox, R. G., Lawrence, P. J., Lichstein, J. W., Longo, M.,  
641 Matheny, A. M., Medvigy, D., Muller-Landau, H. C., Powell, T. L., Serbin, S. P., Sato,  
642 H., Shuman, J. K., Smith, B., Trugman, A. T., Viskari, T., Verbeeck, H., Weng, E., Xu,  
643 C., Xu, X., Zhang, T. and Moorcroft, P. R.: Vegetation demographics in Earth System  
644 Models: A review of progress and priorities, *Glob. Change Biol.*, 24(1), 35–54,  
645 doi:10.1111/gcb.13910, 2018.
- 646 Friend, A. D., Arneth, A., Kiang, N. Y., Lomas, M., Ogee, J., Roedenbeck, C., Running, S. W.,  
647 Santaren, J.-D., Sitch, S., Viogy, N., Woodward, F. I. and Zaehle, S.: FLUXNET and  
648 modelling the global carbon cycle, *Glob. Change Biol.*, 13(3), 610–633,  
649 doi:10.1111/j.1365-2486.2006.01223.x, 2007.
- 650 Gersani, M., Brown, J. s., O'Brien, E. E., Maina, G. M. and Abramsky, Z.: Tragedy of the  
651 commons as a result of root competition, *J. Ecol.*, 89(4), 660–669, doi:10.1046/j.0022-  
652 0477.2001.00609.x, 2001.
- 653 Givnish, T. J.: On the Adaptive Significance of Leaf Height in Forest Herbs, *Am. Nat.*, 120(3),  
654 353–381, doi:10.1086/283995, 1982.



- 655 Haverd, V., Smith, B., Raupach, M., Briggs, P., Nieradzik, L., Beringer, J., Hutley, L.,  
656 Trudinger, C. M. and Cleverly, J.: Coupling carbon allocation with leaf and root  
657 phenology predicts tree–grass partitioning along a savanna rainfall gradient,  
658 *Biogeosciences*, 13(3), 761–779, doi:10.5194/bg-13-761-2016, 2016.
- 659 Hibbs, D. E.: Forty Years of Forest Succession in Central New England, *Ecology*, 64(6), 1394–  
660 1401, doi:10.2307/1937493, 1983.
- 661 Hoffman, F. M., Koven, C. D., Keppel-Aleks, G., Lawrence, D. M., Riley, W. J., Randerson, J.  
662 T., Ahlström, A., Abramowitz, G., Baldocchi, D. D., Best, M. J., Bond-Lamberty, B., De  
663 Kauwe, M. G., Denning, A. S., Desai, A. R., Eyring, V., Fisher, J. B., Fisher, R. A.,  
664 Gleckler, P. J., Huang, M., Hugelius, G., Jain, A. K., Kiang, N. Y., Kim, H., Koster, R.  
665 D., Kumar, S. V., Li, H., Luo, Y., Mao, J., McDowell, N. G., Mishra, U., Moorcroft, P.  
666 R., Pau, G. S. H., Ricciuto, D. M., Schaefer, K., Schwalm, C. R., Serbin, S. P.,  
667 Shevliakova, E., Slater, A. G., Tang, J., Williams, M., Xia, J., Xu, C., Joseph, R. and  
668 Koch, D.: 2016 International Land Model Benchmarking (ILAMB) Workshop Report.,  
669 2017.
- 670 Keenan, T. F., Davidson, E. A., Munger, J. W. and Richardson, A. D.: Rate my data: quantifying  
671 the value of ecological data for the development of models of the terrestrial carbon cycle,  
672 *Ecol. Appl.*, 23(1), 273–286, doi:10.1890/12-0747.1, 2013.
- 673 Koven, C. D., Chambers, J. Q., Georgiou, K., Knox, R., Negron-Juarez, R., Riley, W. J., Arora,  
674 V. K., Brovkin, V., Friedlingstein, P. and Jones, C. D.: Controls on terrestrial carbon  
675 feedbacks by productivity versus turnover in the CMIP5 Earth System Models,  
676 *Biogeosciences*, 12(17), 5211–5228, doi:10.5194/bg-12-5211-2015, 2015.
- 677 Krinner, G., Viovy, N., de Noblet-Ducoudré, N., Ogée, J., Polcher, J., Friedlingstein, P., Ciais,  
678 P., Sitch, S. and Prentice, I. C.: A dynamic global vegetation model for studies of the  
679 coupled atmosphere-biosphere system, *Glob. Biogeochem. Cycles*, 19(1),  
680 doi:10.1029/2003GB002199, 2005.
- 681 Lacointe, A.: Carbon allocation among tree organs: A review of basic processes and  
682 representation in functional-structural tree models, *Ann. For. Sci.*, 57(5), 521–533,  
683 doi:10.1051/forest:2000139, 2000.
- 684 Luo, Y. and Weng, E.: Dynamic disequilibrium of the terrestrial carbon cycle under global  
685 change, *Trends Ecol. Evol.*, 26(2), 96–104, doi:10.1016/j.tree.2010.11.003, 2011.
- 686 Luo, Y., Hui, D. and Zhang, D.: Elevated CO<sub>2</sub> stimulates net accumulations of carbon and  
687 nitrogen in land ecosystems: a meta-analysis, *Ecology*, 87(1), 53–63, 2006.
- 688 Luo, Y. Q., Wu, L. H., Andrews, J. A., White, L., Matamala, R., Schafer, K. V. R. and  
689 Schlesinger, W. H.: Elevated CO<sub>2</sub> differentiates ecosystem carbon processes:  
690 Deconvolution analysis of Duke Forest FACE data, *Ecol. Monogr.*, 71(3), 357–376,  
691 doi:10.1890/0012-9615(2001)071[0357:ECDECP]2.0.CO;2, 2001.
- 692 Luo, Y. Q., Randerson, J. T., Abramowitz, G., Bacour, C., Blyth, E., Carvalhais, N., Ciais, P.,  
693 Dalmonech, D., Fisher, J. B., Fisher, R., Friedlingstein, P., Hibbard, K., Hoffman, F.,  
694 Huntzinger, D., Jones, C. D., Koven, C., Lawrence, D., Li, D. J., Mahecha, M., Niu, S.  
695 L., Norby, R., Piao, S. L., Qi, X., Peylin, P., Prentice, I. C., Riley, W., Reichstein, M.,  
696 Schwalm, C., Wang, Y. P., Xia, J. Y., Zaehle, S. and Zhou, X. H.: A framework for





- 697 benchmarking land models, *Biogeosciences*, 9(10), 3857–3874, doi:10.5194/bg-9-3857-  
698 2012, 2012.
- 699 McCormack, M. L., Guo, D., Iversen, C. M., Chen, W., Eissenstat, D. M., Fernandez, C. W., Li,  
700 L., Ma, C., Ma, Z., Poorter, H., Reich, P. B., Zadworny, M. and Zanne, A.: Building a  
701 better foundation: improving root-trait measurements to understand and model plant and  
702 ecosystem processes, *New Phytol.*, 215(1), 27–37, doi:10.1111/nph.14459, 2017.
- 703 McMurtrie, R. E., Iversen, C. M., Dewar, R. C., Medlyn, B. E., Näsholm, T., Pepper, D. A. and  
704 Norby, R. J.: Plant root distributions and nitrogen uptake predicted by a hypothesis of  
705 optimal root foraging, *Ecol. Evol.*, 2(6), 1235–1250, doi:10.1002/ece3.266, 2012.
- 706 McNickle, G. G. and Dybzinski, R.: Game theory and plant ecology, edited by J. Klironomos,  
707 *Ecol. Lett.*, 16(4), 545–555, doi:10.1111/ele.12071, 2013.
- 708 Menge, D. N. L., Batterman, S. A., Hedin, L. O., Liao, W., Pacala, S. W. and Taylor, B. N.: Why  
709 are nitrogen-fixing trees rare at higher compared to lower latitudes?, *Ecology*, 98(12),  
710 3127–3140, doi:10.1002/ecy.2034, 2017.
- 711 Montané, F., Fox, A. M., Arellano, A. F., MacBean, N., Alexander, M. R., Dye, A., Bishop, D.  
712 A., Trouet, V., Babst, F., Hessel, A. E., Pederson, N., Blanken, P. D., Bohrer, G., Gough,  
713 C. M., Litvak, M. E., Novick, K. A., Phillips, R. P., Wood, J. D. and Moore, D. J. P.:  
714 Evaluating the effect of alternative carbon allocation schemes in a land surface model  
715 (CLM4.5) on carbon fluxes, pools, and turnover in temperate forests, *Geosci. Model*  
716 *Dev.*, 10(9), 3499–3517, doi:10.5194/gmd-10-3499-2017, 2017.
- 717 Moorcroft, P. R., Hurtt, G. C. and Pacala, S. W.: A method for scaling vegetation dynamics: The  
718 ecosystem demography model (ED), *Ecol. Monogr.*, 71(4), 557–585, doi:10.1890/0012-  
719 9615(2001)071[0557:AMFSVD]2.0.CO;2, 2001.
- 720 Nie, M., Lu, M., Bell, J., Raut, S. and Pendall, E.: Altered root traits due to elevated CO<sub>2</sub>: a  
721 meta-analysis: Root traits at elevated CO<sub>2</sub>, *Glob. Ecol. Biogeogr.*, 22(10), 1095–1105,  
722 doi:10.1111/geb.12062, 2013.
- 723 Norby, R. J., Sholtis, J. D., Gunderson, C. A. and Jawdy, S. S.: Leaf dynamics of a deciduous  
724 forest canopy: no response to elevated CO<sub>2</sub>, *Oecologia*, 136(4), 574–584,  
725 doi:10.1007/s00442-003-1296-2, 2003.
- 726 Ordoñez, J. C., van Bodegom, P. M., Witte, J.-P. M., Wright, I. J., Reich, P. B. and Aerts, R.: A  
727 global study of relationships between leaf traits, climate and soil measures of nutrient  
728 fertility, *Glob. Ecol. Biogeogr.*, 18(2), 137–149, doi:10.1111/j.1466-8238.2008.00441.x,  
729 2009.
- 730 Pappas, C., Fatichi, S. and Burlando, P.: Modeling terrestrial carbon and water dynamics across  
731 climatic gradients: does plant trait diversity matter?, *New Phytol.*, 209(1), 137–151,  
732 doi:10.1111/nph.13590, 2016.
- 733 Parton, W., Schimel, D., Cole, C. and Ojima, D.: Analysis of factors controlling soil organic  
734 matter levels in Great Plains grasslands, *Soil Sci. Soc. Am. J.*, 51(5), 1173–1179,  
735 doi:10.2136/sssaj1987.03615995005100050015x, 1987.



- 736 Phillips, R. P., Brzostek, E. and Midgley, M. G.: The mycorrhizal-associated nutrient economy: a  
737 new framework for predicting carbon-nutrient couplings in temperate forests, *New*  
738 *Phytol.*, 199(1), 41–51, doi:10.1111/nph.12221, 2013.
- 739 Raich, J., Rastetter, E. B., Melillo, J. M., Kicklighter, D. W., Steudler, P. A., Peterson, B. J.,  
740 Grace, A., Moore, B. and Vorosmary, C. J.: Potential Net Primary Productivity in South  
741 America: Application of a Global Model, *Ecol. Appl.*, 1(4), 399–429,  
742 doi:10.2307/1941899, 1991.
- 743 Randerson, J., Thompson, M., Conway, T., Fung, I. and Field, C.: The contribution of terrestrial  
744 sources and sinks to trends in the seasonal cycle of atmospheric carbon dioxide, *Glob.*  
745 *Biogeochem. Cycles*, 11(4), 535–560, doi:10.1029/97GB02268, 1997.
- 746 Savage, K. E., Parton, W. J., Davidson, E. A., Trumbore, S. E. and Frey, S. D.: Long-term  
747 changes in forest carbon under temperature and nitrogen amendments in a temperate  
748 northern hardwood forest, *Glob. Change Biol.*, 19(8), 2389–2400,  
749 doi:10.1111/gcb.12224, 2013.
- 750 Scheiter, S. and Higgins, S. I.: Impacts of climate change on the vegetation of Africa: an  
751 adaptive dynamic vegetation modelling approach, *Glob. Change Biol.*, 15(9), 2224–2246,  
752 doi:10.1111/j.1365-2486.2008.01838.x, 2009.
- 753 Scheiter, S., Langan, L. and Higgins, S. I.: Next-generation dynamic global vegetation models:  
754 learning from community ecology, *New Phytol.*, 198(3), 957–969,  
755 doi:10.1111/nph.12210, 2013.
- 756 Schmidt, G. A., Kelley, M., Nazarenko, L., Ruedy, R., Russell, G. L., Aleinov, I., Bauer, M.,  
757 Bauer, S. E., Bhat, M. K., Bleck, R., Canuto, V., Chen, Y.-H., Cheng, Y., Clune, T. L.,  
758 Del Genio, A., de Fainchtein, R., Faluvegi, G., Hansen, J. E., Healy, R. J., Kiang, N. Y.,  
759 Koch, D., Lacis, A. A., LeGrande, A. N., Lerner, J., Lo, K. K., Matthews, E. E., Menon,  
760 S., Miller, R. L., Oinas, V., Olosio, A. O., Perlwitz, J. P., Puma, M. J., Putman, W. M.,  
761 Rind, D., Romanou, A., Sato, M., Shindell, D. T., Sun, S., Syed, R. A., Tausnev, N.,  
762 Tsigaridis, K., Unger, N., Voulgarakis, A., Yao, M.-S. and Zhang, J.: Configuration and  
763 assessment of the GISS ModelE2 contributions to the CMIP5 archive, *J. Adv. Model.*  
764 *Earth Syst.*, 6(1), 141–184, doi:10.1002/2013MS000265, 2014.
- 765 Shevliakova, E., Pacala, S. W., Malyshev, S., Hurtt, G. C., Milly, P. C. D., Caspersen, J. P.,  
766 Sentman, L. T., Fisk, J. P., Wirth, C. and Crevoisier, C.: Carbon cycling under 300 years  
767 of land use change: Importance of the secondary vegetation sink, *Glob. Biogeochem.*  
768 *Cycles*, 23, GB2022, doi:10.1029/2007GB003176, 2009.
- 769 Shinozaki, Kichiro, Yoda, Kyoji, Hozumi, Kazuo and Kira, Tatuo: A quantitative analysis of  
770 plant form – the pipe model theory. I. Basic analyses, *Jpn. J. Ecol.*, 14(3), 97–105, 1964.
- 771 Sierra, C. A. and Mueller, M.: A general mathematical framework for representing soil organic  
772 matter dynamics, *Ecol. Monogr.*, 85(4), 505–524, doi:10.1890/15-0361.1, 2015.
- 773 Sierra, C. A., Muller, M., Metzler, H., Manzoni, S. and Trumbore, S. E.: The muddle of ages,  
774 turnover, transit, and residence times in the carbon cycle, *Glob. Change Biol.*, 23(5),  
775 1763–1773, doi:10.1111/gcb.13556, 2017.
- 776 Sitch, S., Smith, B., Prentice, I. C., Arneeth, A., Bondeau, A., Cramer, W., Kaplan, J. O., Levis,  
777 S., Lucht, W., Sykes, M. T., Thonicke, K. and Venevsky, S.: Evaluation of ecosystem



- 778 dynamics, plant geography and terrestrial carbon cycling in the LPJ dynamic global  
779 vegetation model, *Glob. Change Biol.*, 9(2), 161–185, doi:10.1046/j.1365-  
780 2486.2003.00569.x, 2003.
- 781 Strigul, N., Pristinski, D., Purves, D., Dushoff, J. and Pacala, S.: Scaling from trees to forests:  
782 tractable macroscopic equations for forest dynamics, *Ecol. Monogr.*, 78(4), 523–545,  
783 doi:10.1890/08-0082.1, 2008.
- 784 Tilman, D.: *Plant strategies and the dynamics and structure of plant communities*, Princeton  
785 University Press, Princeton, N.J., 1988.
- 786 Urbanski, S., Barford, C., Wofsy, S., Kucharik, C., Pyle, E., Budney, J., McKain, K., Fitzjarrald,  
787 D., Czikowsky, M. and Munger, J. W.: Factors controlling CO<sub>2</sub> exchange on timescales  
788 from hourly to decadal at Harvard Forest, *J. Geophys. Res. - Biogeosciences*, 112(G2),  
789 doi:10.1029/2006JG000293, 2007.
- 790 Vitousek, P. M., Menge, D. N. L., Reed, S. C. and Cleveland, C. C.: Biological nitrogen fixation:  
791 rates, patterns and ecological controls in terrestrial ecosystems, *Philos. Trans. R. Soc. B*  
792 *Biol. Sci.*, 368(1621), 20130119–20130119, doi:10.1098/rstb.2013.0119, 2013.
- 793 Weng, E., Farrior, C. E., Dybzinski, R. and Pacala, S. W.: Predicting vegetation type through  
794 physiological and environmental interactions with leaf traits: evergreen and deciduous  
795 forests in an earth system modeling framework, *Glob. Change Biol.*, 23(6), 2482–2498,  
796 doi:10.1111/gcb.13542, 2017.
- 797 Weng, E. S., Malyshev, S., Lichstein, J. W., Farrior, C. E., Dybzinski, R., Zhang, T.,  
798 Shevliakova, E. and Pacala, S. W.: Scaling from individual trees to forests in an Earth  
799 system modeling framework using a mathematically tractable model of height-structured  
800 competition, *Biogeosciences*, 12(9), 2655–2694, doi:10.5194/bg-12-2655-2015, 2015.
- 801 Xia, J., Luo, Y., Wang, Y.-P. and Hararuk, O.: Traceable components of terrestrial carbon  
802 storage capacity in biogeochemical models, *Glob. Change Biol.*, 19(7), 2104–2116,  
803 doi:10.1111/gcb.12172, 2013.
- 804 Zea-Cabrera, E., Iwasa, Y., Levin, S. and Rodríguez-Iturbe, I.: Tragedy of the commons in plant  
805 water use, *Water Resour. Res.*, 42(6), W06D02, doi:10.1029/2005WR004514, 2006.
- 806